# Rigorous numerical modeling of scattering-type scanning near-field optical microscopy and spectroscopy

Xinzhong Chen,[1] Chiu Fan Bowen Lo,[1] William Zheng,[2] Hai Hu,[3] Qing Dai,[3,a)] and Mengkun Liu[1,a)]
[1]*Department of Physics and Astronomy, Stony Brook University, Stony Brook, New York 11794, USA*
[2]*Department of Physics, Columbia University, New York, New York 10027, USA*
[3]*Division of Nanophotonics, CAS Center for Excellence in Nanoscience, National Center for Nanoscience and Technology, Beijing 100190, People's Republic of China*

(Received 9 October 2017; accepted 12 November 2017; published online 1 December 2017)

Over the last decade, scattering-type scanning near-field optical microscopy and spectroscopy have been widely used in nano-photonics and material research due to their fine spatial resolution and broad spectral range. A number of simplified analytical models have been proposed to quantitatively understand the tip-scattered near-field signal. However, a rigorous interpretation of the experimental results is still lacking at this stage. Numerical modelings, on the other hand, are mostly done by simulating the local electric field slightly above the sample surface, which only qualitatively represents the near-field signal rendered by the tip-sample interaction. In this work, we performed a more comprehensive numerical simulation which is based on realistic experimental parameters and signal extraction procedures. By directly comparing to the experiments as well as other simulation efforts, our methods offer a more accurate quantitative description of the near-field signal, paving the way for future studies of complex systems at the nanoscale. *Published by AIP Publishing.*
https://doi.org/10.1063/1.5008663

Recent development in scattering-type scanning near-field optical microscopy (s-SNOM) has initiated a wide range of new research activities in condensed matter physics and nanophotonics. s-SNOM is capable of achieving a 10 nm spatial resolution which is practically independent of the illumination wavelength. It has a wide range of applications including imaging solid-solid phase transition and phase inhomogeneities in strongly correlated electron materials,[1–5] mapping surface plasmon or phonon polariton wave propagation in 2D van der Waals microcrystals,[6–9] probing electromagnetic modes in plasmonic nanostructures,[10–12] and much more.[13–15]

Like any scanning probe method, the interpretation of the tip-sample interactions in s-SNOM requires a stringent theoretical treatment. A number of analytical models have been proposed to quantify the tip-scattered near-field signal, ranging from the most straightforward momentum-dependent $r_p$ calculation at the quasistatic limit,[16] point-dipole approximation,[17,18] to the more mathematically involved elongated spheroid model.[19–21] These analytical models are either too simplified or become computationally expensive very quickly. More importantly, most of the available analytical models are based on the assumption that the sample has an infinite lateral size, which cannot address nanoscale inhomogeneities and geometric factors in the sample.

To address the sample inhomogeneity, simplified numerical simulations, in which the near-surface electric field (NSEF) is used to represent the near-field scattering signal, have been routinely practiced.[22–24] However, the assumption that the detected near-field signal is directly proportional to the NSEF is only qualitatively valid. In this work, we demonstrate an advanced numerical simulation approach that has the capability to achieve quantitative consistency with experimental data without extreme mathematical complexities and ad-hoc assumptions.

We first discuss the optical layout and signal acquisition process in a typical s-SNOM system. In a standard setup (Fig. 1), an atomic force microscope (AFM) provides the basic scanning probe platform with sample scanning and sample approaching. The AFM probe, typically a sharp tip coated with reflective metal, is vibrating vertically on top of the sample surface with a typical magnitude of 40–100 nm. An illumination light source, either monochromatic or broadband, is focused, commonly by a parabolic mirror, onto the AFM tip area with an incident angle of 55°–65° with respect to the surface normal. The light scattered by the tip-sample system is collected by a fast detector, and the signal is sent to a lock-in amplifier with multiple frequency demodulators. By making use of a Michaelson interferometry setup, both amplitude and phase of the scattered signal can be resolved. The tip is vibrating harmonically in the vertical direction so that the scattered optical signal is modulated by the tip

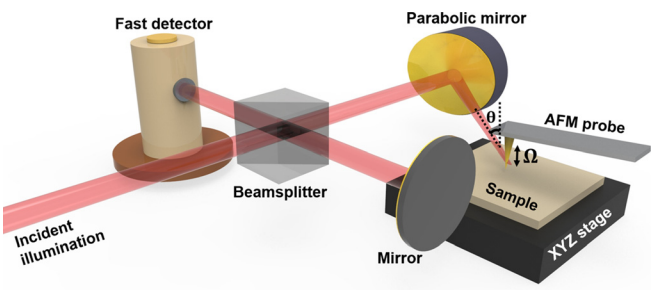


FIG. 1. Schematics of a typical s-SNOM setup. The reference mirror is sitting on a delay stage (not shown).

a)Electronic mail: daiq@nanoctr.cn and mengkun.liu@stonybrook.edu

oscillation. After demodulating the detected signal at higher harmonics of the oscillation frequency, the "far-field" background is greatly suppressed and the genuine near-field information is preserved. Detailed introduction to the s-SNOM experimental setup can be found in previous works done by Patane *et al*. and Keilmann and Hillenbrand in 2004.[25,26]

In a near-field imaging experiment, a monochromatic laser is often used as the light source. The sample stage raster scans over an area whose size is typically in the order of 1 to 10 $\mu$m while the fast detector registers the scattered signal at each pixel. After demodulation, background-free near-field images can be constructed. On the other hand, near-field infrared spectroscopy (nano-FTIR) is a unique combination of s-SNOM and conventional far-field Fourier transformed infrared spectroscopy (FTIR).[27] A broadband light source like synchrotron infrared (IR) source can be coupled to the s-SNOM system. While the sample is stationary, the reference mirror scans over a spatial range so that an interferogram is formed. Finally, the frequency domain near-field spectrum is calculated simply by Fourier transforming the interferogram.

We use a commercial software (CST microwave studio) to perform numerical simulations of the above signal acquisition process. The advantages of commercial solvers include easy-to-use modeling platform, preprogrammed finite-difference time-domain (FDTD) and finite element method (FEM) algorithms, and a wide range of adjustable parameters and material database. Based on CST, we model the s-SNOM experiments in a realistic manner. The tip is modeled as a truncated gold cone with a bottom radius of 30 nm, a top radius of 100 nm, and a length of 1 $\mu$m. A gold hemisphere of 30 nm radius is added to the bottom of the cone to mimic the tip apex. Samples with specific geometric and dielectric properties can be modeled accordingly under the tip. The sizes of the sample, the boundary box, and the tip are chosen so that the simulation will yield a genuine tip-sample response while at the same time minimize the computation time. By searching the parameter space, we find that a lateral size of 2–3 $\mu$m and a thickness of 300–500 nm are optimal for most of the samples we study. Due to the singularity at the tip apex, we use a relatively large number of mesh cells to resolve the detailed features. Usually, the total number of mesh cells in a model is between one and three million. For this reason, a typical simulation of one spectrum or one pixel point in the image takes a standard desktop computer several hours.

The schematic illustration of the simulation model is shown in Fig. 2(a). For convenience, we use two coordinate systems: a model coordinate $xyz$ and a sample coordinate $x'y'z'$. The model coordinate system is set up such that the incident illumination and back-scattered detection are from the front $yz$ plane, which is a waveguide port for both illumination and detection. The sample surface ($x'y'$ plane) has an angle of 30°–35° with respect to the $xy$ plane, which simulates the 55°–60° incident angle in a typical experimental setup. Open boundary conditions are used on front and back $yz$ planes, and $E_t = 0$ ($H_t = 0$) is used on $xy$ ($xz$) planes, where $E_t$ and $H_t$ represent the tangential components of the electric field and magnetic field, respectively. Those boundary conditions ensure a p-polarized incident planewave. Due to the finite sizes of the simulation, there are artificial hot spots caused by the sample edges and boundaries [Fig. 2(b)].

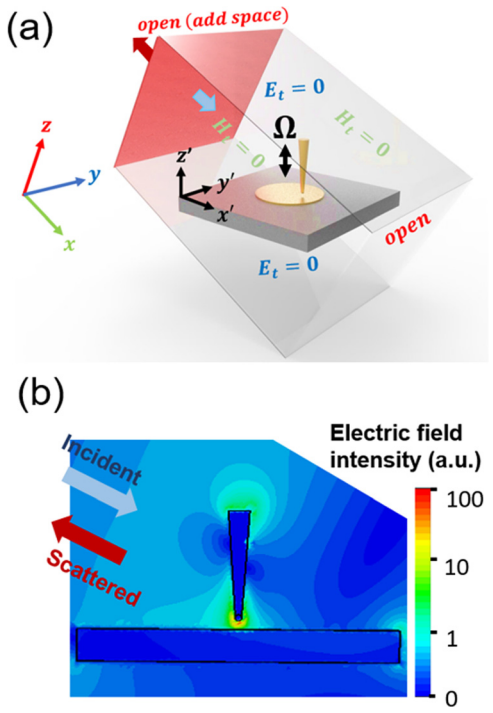


FIG. 2. (a) A plane wave port with polarized boundary conditions in CST. (b) Simulated electric-field intensity distribution.

Fortunately, as we will demonstrate below, those artifacts will be elegantly eliminated by the demodulation procedure since they do not have a strong nonlinear dependence on the tip-sample distance.

In our model, the distance between the tip and the sample surface is given by a harmonic motion

$$z = A - A\cos(\omega t), \tag{1}$$

where $A$ is the oscillation amplitude and $\omega$ is the angular frequency of the tip tapping motion. In a typical experimental setup, the tapping magnitude ($2A$) is between 40 and 80 nm and the tapping frequency $f = \omega/2\pi$ is in the order of 100 kHz.

To facilitate the simulation, we discretize $z$ into $N$ steps from $z = 0$ nm to $z = 2A$. $N$ is typically 10 to 15. Since the tip-sample interaction increases dramatically as the tip is closer to the sample, a finer step is usually used when $z$ is small. For each $z$ value, a reflection spectrum is simulated in the time domain solver (FDTD). The frequency domain solver (FEM) can also be used to yield similar results, but it is more time consuming. Let $r(z,f)$ be the frequency ($f$) dependent complex reflection spectrum at the tip-sample distance $z$. After $N$ steps, we obtain a total of $N$ spectra, which can be labeled as $r(z_1,f)$, $r(z_2,f)$, $r(z_3,f)$,…, $r(z_N,f)$. These far-field spectra are not particularly of interest because they represent a complex mixture of tip and sample reflections which also contain artefacts posted by the finite boundaries in our model. However, as previously mentioned, in experiments, the detected tip scattered signal is demodulated at higher harmonics of the tip oscillation frequency to suppress undesired background and preserve only the near-field signals. In the case of our simulations, this demodulation procedure also eliminates undesired background and artifacts

imbedded in the model geometry. This demodulation procedure can be expressed as

$$S_n(f) \propto \int_0^T r(t,f)e^{-in\omega t}dt, \tag{2}$$

where $S_n(f)$ represents the complex $n$ th-harmonics near-field signal and $T = \frac{2\pi}{\omega}$ is the tip oscillation period. We note that the integral in Eq. (2) is over one period in our calculation, but in experiments, the detected signal is integrated over many periods to achieve a reduced noise level. The ratio between the near-field signal and undesired background decreases exponentially as $n$ increases, but the overall signal level also decreases with increasing $n$.[28] Therefore, in actual experiments and here in simulation as well, $n = 2$ and 3 are often used. Equation (2) is a finite time integral and our simulation is performed in discrete $z$ values; $t$ as a function of $z$ can be written as

$$t_N = \frac{1}{\omega}\arccos\left(\frac{A - z_N}{A}\right) \tag{3}$$

and $S_n(f)$ as

$$S_n(f) \propto \sum_N r(t_N,f)\mathrm{e}^{-in\omega t_N}(t_{N+1} - t_N), \tag{4}$$

which allows us to calculate the 2nd and 3rd harmonic near-field signals $S_2$ and $S_3$. Modeling the AFM tip as a truncated metallic cone or similar geometries has been demonstrated in previous efforts of s-SNOM simulations.[29,30] However, combining both the realistic tip modeling and the higher harmonic signal demodulation as a background suppression technique is not yet implemented in previous studies to yield the genuine complex near-field signal. In the following, we discuss simulations of near-field spectroscopy and nano-imaging and compare our demodulation-based tip-modeling (DBTM) method to experimental results and previously practiced NSEF simulations.

We first present the nano-spectroscopic investigations of hexagonal Boron Nitride (hBN) and $SiO_2$ in the mid-IR frequency ranges where distinct IR active phonon responses are present. The near-field phonon dispersion is usually the most difficult regime to deal with numerically, due to the rapid change of dielectric constants in a relatively small frequency window. Nevertheless, the DBTM simulations demonstrate good agreement with the experimental data, which are shown in Figs. 3(a) and 3(b). Nano-FTIR experiments are performed on a 1800 nm hBN flake and a 300 nm $SiO_2$/Si wafer at Advanced Light Source, Berkeley (SINS). Compared to the DBTM simulations, NSEF simulation of hBN (not shown) deviates significantly from experimental observation, and NSEF simulation of $SiO_2$ is only qualitatively consistent as shown in Fig. 3(b). All the spectra in Fig. 3 are normalized to their own peak values for easier comparison. Spectra in Fig. 3(a) are smoothed with a moving average filter for better presentation. It is clear that the near-surface electric field intensity only qualitatively maps onto the near-field spectroscopy data-although the peak feature sometimes can be captured. Noticeably, NSEF with tip included in the model (without demodulation) yields slightly better consistency than that without a tip.

To demonstrate the robustness of our methods, we also investigate the relationship between the demodulated near-field signal and the incident/detection angle. It has long been practiced experimentally that an incident angle of 55°–65° yields optimal $S_2$ and $S_3$ signals. Here, we use the peak amplitude of $SiO_2$ phonon at $\sim$1130 $cm^{-1}$ as a cursor and perform

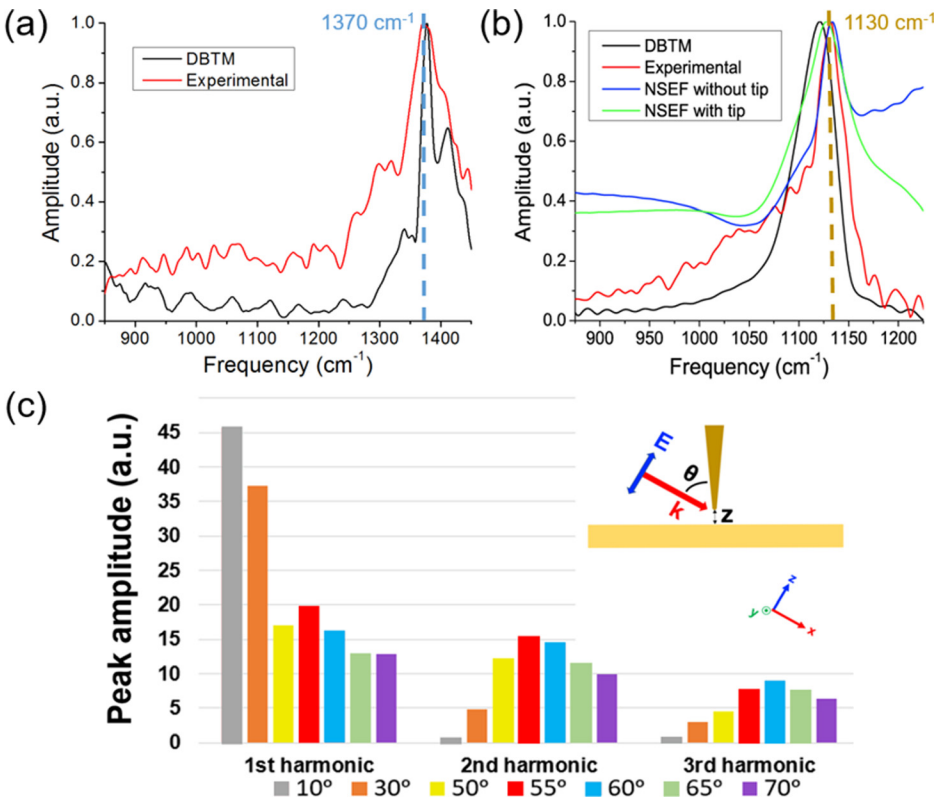


FIG. 3. (a) and (b) Experimentally measured hBN $S_2$ (a) and $SiO_2$ $S_3$ (b) spectra (red) along with simulated spectra given by DBTM (black), NSEF without tip (blue), and NSEF with tip (green). The NSEF simulation for hBN is not shown here since they do not show presentable features. Phonon peaks are indicated by dashed lines. (c) Angle dependence of the demodulated signal amplitudes of the 1st to 3rd harmonics, at the peak of the $SiO_2$ phonon frequency.

simulations at different incident angles. The results are shown in Fig. 3(c). It clearly verifies that for $S_2$ and $S_3$, an incident angle of 55°–65° is optimal, consistent with experiments. It also reveals that for the 1st harmonics, a small incident angle (close to normal incident) leads to a larger signal level, which is not surprising since the 1st harmonics signal contains a significant far-field background.

Nano-imaging can be simulated using the same setup and mathematical procedure as in the spectrum simulation. The only difference is that when simulating an image, the tip oscillates in the $z$ direction and the sample raster scans across the $x'y'$ plane. In addition, a good quality near-field imaging is usually performed with monochromatic light illumination. The capability to quantitatively simulate near-field contrast in an inhomogeneous sample is the major advantage of the proposed simulation method as all the current analytical models assume the sample to be a homogeneous infinite half space.

The simulation results of a near-field line scan across a gold disk on a sapphire substrate are shown in Fig. 4(a). The gold disk has a radius of 650 nm and a thickness of 30 nm. Experimentally, the disk is measured with a Quantum Cascade Laser (QCL) at a wavelength of ~6 $\mu$m [Fig. 4(b)]. To perform the simulation, the tip is fixed at position $(x, y)$ in the sample coordinate system. The tip-sample distance follows the same motion as in Eq. (1). The disk is moved with small steps at a time so that the tip is at $(x_0 + dx, y_0)$ relative to the disk and the simulation repeats. Moving the disk (not the tip) agrees with the experimental procedure and helps reduce boundary artefacts in the simulation. A symmetry plane along the x' direction can also be implemented to reduce the calculation time. Since a monochromatic light illumination is used, instead of $S_n(f)$, we get $S_n(x, y)$. Once again, our simulation is capable of reproducing this pattern with decent agreement and a high spatial resolution can be readily obtained at the edge of the disk. The mechanism of this near-field pattern formation in plasmonic disks is discussed in Ref. 11.

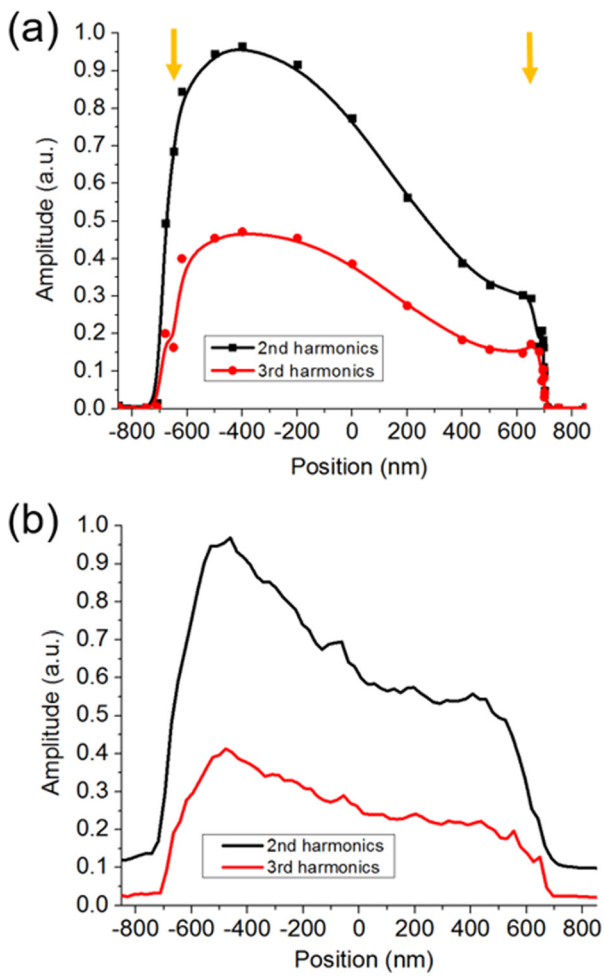


FIG. 4. (a) Simulated and (b) measured line scan profiles of near-field second ($S_2$) and third harmonics ($S_3$) of a gold disk (radius ~650 nm) on the sapphire substrate with 6 $\mu$m incident light. The yellow arrow indicates the physical boundary of the gold disk.

In the end, we provide one prediction on the s-SNOM contrast between gold and sapphire in the terahertz (THz) frequency regime. Operating s-SNOM in the THz range is one of the most exciting research forefronts. THz s-SNOM imaging and spectroscopy have been previously demonstrated experimentally.[31,32] However, due to the technical difficulties in generating and detecting intense coherent THz light, THz s-SNOM has not achieved an excellent signal to noise ratio compared to IR s-SNOMs. With DBTM simulations using a longer tip and larger sample geometry, we conclude that the THz near-field signal amplitude in gold is roughly 2–3-fold of that in sapphire for $S_3$, at ~1 THz frequency. The prediction awaits future experimental verification.

In summary, we demonstrate a combined numerical and experimental study to simulate near-field spectroscopy and microscopy measurements. Compared to the previous efforts,[22–24,33] our methods include realistic tip geometry, tip-sample interactions, and proper signal processing procedure. Superior agreements between our methods and the experimental data illustrate the importance of the tip-sample distance modulations for understanding the near-field data. With an improved computation power, the time efficiency can be further improved and this approach can be modified to study other aspects of the near-field related problems. For example, optimal tip geometry can be tested, especially in the THz regime where the length of the tip is considered to be of great importance due to the antenna effect. The far-field associated effect with the multiple reflections between the sample and the tip can also be addressed and insightful conclusions can be drawn to guide future experiments.

The authors would like to acknowledge Hans Bechtel and Michael Martin for setting up the s-SNOM system for nano-FTIR and nano-imaging experiments at Lawrence Berkeley National Laboratory (SINS beamline). The authors also would like to acknowledge Kebin Fan for the discussions on designing the CST simulation.

[1]M. Liu, A. J. Sternbach, and D. N. Basov, Rep. Prog. Phys. **80**, 14501 (2017).
[2]A. S. McLeod, E. van Heumen, J. G. Ramirez, S. Wang, T. Saerbeck, S. Guenon, M. Goldflam, L. Anderegg, P. Kelly, A. Mueller, M. K. Liu, I. K. Schuller, and D. N. Basov, Nat. Phys. **13**, 80 (2017).
[3]A. Charnukha, A. Cvitkovic, T. Prokscha, D. Pröpper, N. Ocelic, A. Suter, Z. Salman, E. Morenzoni, J. Deisenhofer, V. Tsurkan, A. Loidl, B. Keimer, and A. V. Boris, Phys. Rev. Lett. **109**(1), 017003 (2012).
[4]A. C. Jones, S. Berweger, J. Wei, D. Cobden, and M. B. Raschke, Nano Lett. **10**, 1574 (2010).

[5]M. K. Liu, M. Wagner, E. Abreu, S. Kittiwatanakul, A. McLeod, Z. Fei, M. Goldflam, S. Dai, M. M. Fogler, J. Lu, S. A. Wolf, R. D. Averitt, and D. N. Basov, Phys. Rev. Lett. **111**, 96602 (2013).
[6]Z. Fei, M. D. Goldflam, J. S. Wu, S. Dai, M. Wagner, A. S. McLeod, M. K. Liu, K. W. Post, S. Zhu, G. C. A. M. Janssen, M. M. Fogler, and D. N. Basov, Nano Lett. **15**, 8271 (2015).
[7]J. Ehlermann, S. Fohrmann, J. Siebels, and S. Mendach, Phys. Rev. B **91**, 235404 (2015).
[8]G. X. Ni, L. Wang, M. D. Goldflam, M. Wagner, Z. Fei, A. S. McLeod, M. K. Liu, F. Keilmann, B. Özyilmaz, A. H. Castro Neto, J. Hone, M. M. Fogler, and D. N. Basov, Nat. Photonics **10**, 244 (2016).
[9]L. Gilburd, X. G. Xu, Y. Bando, D. Golberg, and G. C. Walker, J. Phys. Chem. Lett. **7**, 289 (2016).
[10]R. Hillenbrand and F. Keilmann, Appl. Phys. Lett. **80**, 25 (2002).
[11]J. Chen, P. Albella, Z. Pirzadeh, P. Alonso-González, F. Huth, S. Bonetti, V. Bonanni, J. Åkerman, J. Nogués, P. Vavassori, A. Dmitriev, J. Aizpurua, and R. Hillenbrand, Small **7**, 2341 (2011).
[12]A. J. Huber, J. Wittborn, and R. Hillenbrand, Nanotechnology **21**, 235702 (2010).
[13]S. Berweger, D. M. Nguyen, E. A. Muller, H. A. Bechtel, T. T. Perkins, and M. B. Raschke, J. Am. Chem. Soc. **135**, 18292 (2013).
[14]A. A. Govyadinov, S. Mastel, F. Golmar, A. Chuvilin, P. S. Carney, and R. Hillenbrand, ACS Nano **8**, 6911 (2014).
[15]H. Amrania, W. Hart, L. Drummond, C. R. Coombes, S. Shousha, L. N. Woodley, K. Weir, I. Carter, and C. Phillips, Faraday Discuss. **187**, 539 (2016).
[16]S. Dai, Z. Fei, Q. Ma, A. S. Rodin, M. Wagner, A. S. McLeod, M. K. Liu, W. Gannett, W. Regan, K. Watanabe, T. Taniguchi, M. Thiemens, G. Dominguez, A. H. C. Neto, A. Zettl, F. Keilmann, P. Jarillo-Herrero, M. M. Fogler, and D. N. Basov, Science **343**, 1125 (2014).
[17]R. Hillenbrand and F. Keilmann, Phys. Rev. Lett. **85**, 3029 (2000).
[18]R. Hillenbrand, B. Knoll, and F. Keilmann, J. Microsc. **202**, 77 (2001).
[19]A. S. McLeod, P. Kelly, M. D. Goldflam, Z. Gainsforth, A. J. Westphal, G. Dominguez, M. H. Thiemens, M. M. Fogler, and D. N. Basov, Phys. Rev. B **90**, 085136 (2014).
[20]B.-Y. Jiang, L. M. Zhang, A. H. Castro Neto, D. N. Basov, and M. M. Fogler, J. Appl. Phys. **119**, 54305 (2016).
[21]A. Cvitkovic, N. Ocelic, and R. Hillenbrand, Opt. Express **15**, 8550 (2007).
[22]J. A. Schuller, E. S. Barnard, W. Cai, Y. C. Jun, J. S. White, and M. L. Brongersma, Nat. Mater. **9**, 193 (2010).
[23]J. Robertson, Eur. Phys. J. Appl. Phys. **28**, 265 (2004).
[24]D.-S. Kim and Z. H. Kim, Opt. Express **20**, 8689 (2012).
[25]S. Patane, P. G. Gucciardi, M. Labardi, and M. Allegrini, Riv. Nuovo Cimento **27**, 1 (2004).
[26]F. Keilmann and R. Hillenbrand, Philos. Trans. A Math. Phys. Eng. Sci. **362**, 787 (2004).
[27]P. R. Griffiths and J. A. Haseth, *Fourier Transform Infrared Spectrometry*, 2nd ed. (Wiley-Interscience, 2007).
[28]N. Maghelli, M. Labardi, S. Patanè, F. Irrera, and M. Allegrini, J. Microsc. **202**, 84 (2001).
[29]F. Bilotti, S. Tricarico, F. Pierini, and L. Vegni, Opt. Lett. **36**, 211 (2011).
[30]W. Chen, A. Kimel, A. Kirilyuk, and T. Rasing, Phys. Status Solidi (B) **247**, 2047 (2010).
[31]A. J. Huber, F. Keilmann, J. Wittborn, J. Aizpurua, and R. Hillenbrand, Nano Lett. **8**, 3766 (2008).
[32]H.-G. von Ribbeck, M. Brehm, D. W. van der Weide, S. Winnerl, O. Drachenko, M. Helm, and F. Keilmann, Opt. Express **16**, 3430 (2008).
[33]A. García-Etxarri, I. Romero, F. J. García De Abajo, R. Hillenbrand, and J. Aizpurua, Phys. Rev. B. **79**, 125439 (2009).